Metal-insulator transition in the hollandite $K_2V_8O_{16}$ with a frustrated zigzag ladder probed by ^{51}V NMR

Yasuhiro Shimizu,[1,2] Katsunori Okai,[1] Masayuki Itoh,[1] Masahiro Isobe,[3] Jun-Ichi Yamaura,[3] Touru Yamauchi,[3] and Yutaka Ueda[3]

[1]*Department of Physics, Graduate School of Science, Nagoya University, Furo-cho, Chikusa-ku, Nagoya 464-8602, Japan*

[2]*Institute for Advanced Research, Nagoya University, Furo-cho, Chikusa-ku, Nagoya 464-8601, Japan*

[3]*Institute for Solid State Physics, University of Tokyo, Kashiwa, Chiba 277-8581, Japan*

(Received 17 December 2010; revised manuscript received 22 February 2011; published 13 April 2011)

We report the experimental results of ^{51}V NMR measurements on the hollandite $K_2V_8O_{16}$ consisting of a frustrated zigzag ladder with the orbital degrees of freedom. The metal-insulator transition is found to involve the spin-singlet formation by the ^{51}V Knight shift K, the nuclear spin-lattice relaxation rate $1/T_1$, and the spin-echo decay rate $1/T_2$ measurements. In the insulating state, the anisotropic electric-field gradient supports the d_{xy} orbital order with the spin singlet along the chain. The d_{xy} orbital is magnetically most active in the metallic state, as observed by the anisotropic Knight shift, which suggests the strong electron correlation in the d_{xy} band. Despite the large enhancement of the spin susceptibility, no apparent spin correlation is developed in the frustrated metallic state. Pressure suppresses the electron correlation continuously, as highlighted in the decrease of the metal-insulator transition and the spin susceptibility keeping the largest d_{xy} contribution in the metallic state. A robust spin-singlet insulating phase with the large spin gap and paramagnetic spins appears above 1 GPa, which suggests a competition of the charge-orbital ordering pattern.

DOI: 10.1103/PhysRevB.83.155111 PACS number(s): 71.30.+h, 76.60.−k, 75.50.−y, 75.40.Gb

I. INTRODUCTION

Unusual metal-insulator transitions (MIT) and non-Fermi-liquid behavior of geometrically frustrated materials are attractive current issues of active research in strongly correlated electron systems. Examples include the three-dimensional (3D) spinel oxides, e.g., AV_2O_4 (A = Li, Al, Zn, etc.), having the ground states such as the spin-singlet, ferrimagnet, spin ice, and heavy-mass Fermi liquid.[1,2] In the low-dimensional case, such as a zigzag ladder, fluctuations can be enhanced and more favor the quantum liquid state. Indeed, a Heisenberg model of the zigzag ladder predicts degenerated ground states, including nematic,[3,4] topological,[5] chiral,[6] incommensurate magnetic orders,[7] the spin-Bose metal,[8] and the field-induced orbital current.[9] In the presence of the orbital degrees of freedom with the moderate electron correlation and the electron-phonon coupling, various phase transitions have been found, such as the valence bond[10,11] and ferromagnetic[12] orders in hollandites $A_2M_8O_{16}$, and the antiferromagnetic metal[13] and insulator[14] in pyroferites AM_2O_4, where A are alkaline metals and M are transition metals. To understand these phase transitions, the electron correlation and the orbital occupancy would be the dominant parameters, which should be revealed experimentally.

Among the zigzag ladder systems, $K_2V_8O_{16}$ is attractive because of the possible valence-bond crystallization induced by an interplay between spin, charge, orbital, and lattice degrees of freedom.[11] The tetragonal $I4/m$ crystal structure of $K_2V_8O_{16}$ consists of a framework of four double chains holding K ions in a large tunnel, as shown in Figs. 1(a) and 1(b). The interaction within the double chain running along the c axis forms a zigzag ladder of the edge-sharing VO_6. The $3d^{1.25}$ electrons on average (V^{3+} : V^{4+} = 1 : 3) partially occupy the t_{2g} manifold consisting of the d_{yz}-d_{zx} doublet and the d_{xy} singlet,[15,16] as schematically illustrated in Fig. 1(c), and hence the orbital degree of freedom is still active. The MIT occurs at T_{MI} = 160–170 K and accompanies a first-order structural transition from a tetragonal to a monoclinic lattice.[11] Around T_{MI}, the magnetic susceptibility χ_{bulk} of the powder sample continuously decreases, but a large finite value remains.[11] Observations of the $\sqrt{2}a \times \sqrt{2}a \times 2c$ superstructure peaks in the x-ray diffraction imply a charge order with one V^{3+} chain and three V^{4+} chains,[11] suggesting orbital ordering and spin-singlet clusterization. An alternative charge-order pattern with the nonmagnetic and paramagnetic spins was proposed theoretically.[16] Thus the microscopic spin, charge, and orbital states remain unsolved. Applying low pressures, T_{MI} is sensitively suppressed up to 1 GPa, but turns to increase at high pressures up to 7 GPa,[17] implying the competing ground states due to the geometrical frustration.

In this paper, we investigate the local spin susceptibility by the ^{51}V NMR measurements on the high-quality samples of $K_2V_8O_{16}$ at ambient pressure and under pressure. In Sec. III, first we characterize the MIT based on the ^{51}V Knight shift K measurements for a polycrystalline sample, giving the microscopic evidence for the spin-singlet formation. Second, we examine the orbital state based on the anisotropy of the ^{51}V hyperfine coupling tensor and electric-field gradient via the single-crystal experiments. Third, the dynamical properties across the MIT are probed via the nuclear spin-lattice relaxation rate $1/T_1$ and the spin-echo decay rate $1/T_2$ measurements, which confirm the spin-singlet ground state without long-range magnetic order. In Sec. IV, we discuss the spin correlation of the metallic state and the phase diagram of MIT.

II. EXPERIMENT

^{51}V NMR measurements were performed for the polycrystalline and the single-crystal samples of $K_2V_8O_{16}$ made

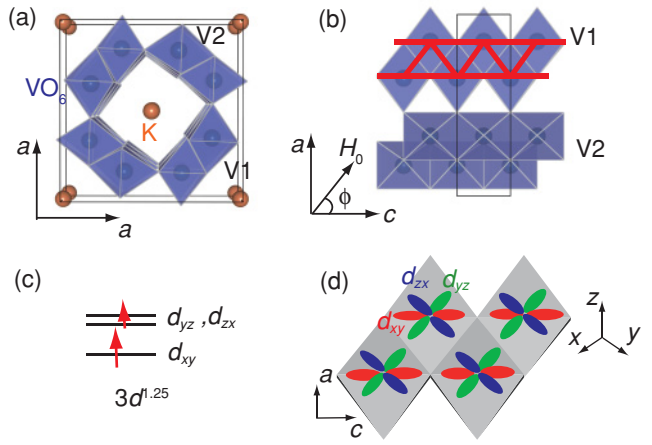

FIG. 1. (Color online) Crystal structure of $K_2V_8O_{16}$ viewed along the (a) c axis or (b) a axis. (c) V t_{2g} levels filled with 1.25 $3d$ electrons on average. (d) Schematics of t_{2g} orbitals in the VO_6 octahedra with the local coordination axes.

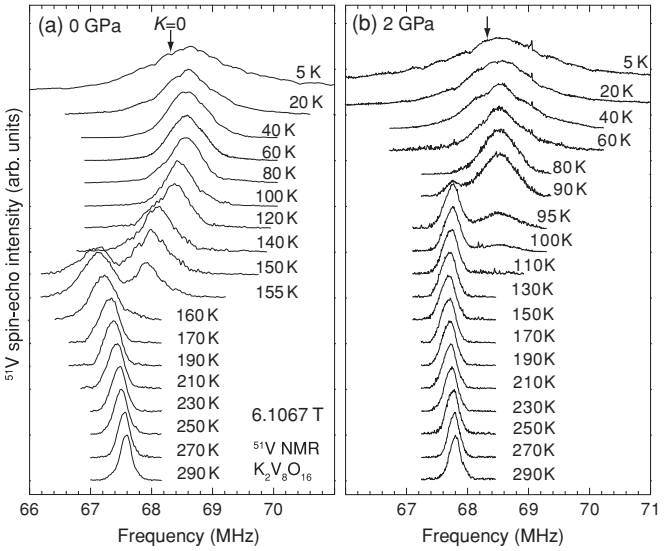

FIG. 2. Temperature dependence of ^{51}V NMR spectra in $K_2V_8O_{16}$, obtained for the polycrystalline sample at (a) ambient pressure and (b) 2 GPa. The spectral intensity is normalized by the maximum value at each temperature.

by a solid-state reaction of KVO_3, V_2O_3, and V_2O_5 under 4 GPa in a cubic-anvil-type pressure cell at 1473 K.[11] Crystallographic axes of the single crystal were determined by x-ray-diffraction measurements. Since the size of the crystal ($0.5 \times 0.1 \times 0.1$ mm) was not enough to gain a sufficient signal-to-noise ratio, we used the polycrystalline sample for the temperature-T dependence measurements. We applied hydrostatic pressure up to 2 GPa in Daphne 7373 oil by using a double-cylinder cell made of BeCu and NiCrAl alloys with a manometer of Cu_2O. Frequency-swept ^{51}V NMR spectra were obtained by the Fourier transformation of the spin-echo signals in a constant magnetic field $H_0 = 6.1067$ T. We defined K as a relative shift from the ^{51}V resonance frequency of an aqueous solution of $NaVO_3$, $\nu_0 = 68.352$ MHz. The angle dependence of K was measured in the single crystal by using a two-axis goniometer at ambient pressure and 1.5 GPa. The spectral intensity and the $\pi/2$ pulse width were strongly dependent on the magnetic field direction due to the anisotropic $1/T_2$. We obtained $1/T_1$ from a single-exponential recovery after an inversion pulse in the metallic phase, and from a stretched-exponential recovery in the insulating phase.

III. EXPERIMENTAL RESULTS

A. Local spin susceptibility

Figure 2(a) displays the T dependence of ^{51}V NMR spectra for the polycrystalline $K_2V_8O_{16}$ at ambient pressure. The single NMR spectrum at 290 K is consistent with only one crystallographically equivalent V site. The symmetric line shape distinct from the so-called asymmetric powder pattern is attributable to the strong signal intensity at certain magnetic field directions, as will be shown in the single-crystal experiments. As the sample is cooled from 290 K, the spectrum shifts to lower frequencies despite an increase of the bulk magnetic susceptibility $\chi_{\rm bulk}$,[11] which indicates a negative hyperfine coupling constant due to the predominant core polarization. The spectrum broadens with the Knight shift with decreasing T.

Below $T_{\rm MI} \sim 155$–160 K, another spectrum, expected to arise from the insulating phase, appears at a higher frequency, and the spectrum from the metallic phase disappears below 140 K. The spectrum from the insulating phase moves to higher frequencies, indicating a decrease of χ_s, and then stays at the frequency slightly higher than the $K = 0$ position below 80 K. It clearly indicates that the spectrum comes from the nonmagnetic V sites. Nevertheless, the spectrum is broad compared to that of the metallic state, which is attributable to the electric quadrupole interaction under the asymmetric electric-field gradient due to the $3d$ orbital order, as discussed in Sec. III B. The further broadening is observed at low temperatures below 20 K without a paramagnetic shift of the central peak. A large distribution of the inhomogeneous local fields reaching ± 3 MHz (± 3 kOe) cannot be attributed to the transferred fields from paramagnetic spins, but to the tiny staggered moments induced around the impurity spins of a few percent observed in $\chi_{\rm bulk}$.

We plot in Fig. 3(a) the T dependence of $-K$ defined by the peak position of the spectrum. In $3d$ systems, K is expressed as a sum of the spin term K_s and the T-invariant Van-Vleck orbital term $K_{\rm orb}$,

$$K = K_s + K_{\rm orb} = \frac{1}{N\mu_{\rm B}}(A_s\chi_s + A_{\rm orb}\chi_{\rm orb}), \qquad (1)$$

using the Avogadro's number N, the Bohr magneton $\mu_{\rm B}$, the Van-Vleck orbital susceptibility $\chi_{\rm orb}$, the spin hyperfine coupling constant A_s, and the orbital one $A_{\rm orb} = 2\mu_{\rm B}\langle r^{-3}\rangle = 446$ kOe/$\mu_{\rm B}$, where the average of $\langle r^{-3}\rangle$ is taken for V^{3+} (3.21 a.u.) : V^{4+} (3.684 a.u.) [Ref. 18] = 1 : 3. The increase of $-K$ is proportional to $\chi_{\rm bulk}$ reported previously[11] in the T range of 170–290 K, as seen in the K-$\chi_{\rm bulk}$ plot of Fig. 4. The linearity of the K-$\chi_{\rm bulk}$ plot, and the intersection with the dotted line $K = A_{\rm orb}\chi_{\rm bulk}$, yield $A_s = -80$ kOe/$\mu_{\rm B}$ and $K_{\rm orb} = 0.45\%$, respectively. After subtracting $K_{\rm orb}$ from K, $-1/K_s$ is plotted against T in Fig. 3(b), to parametrize the

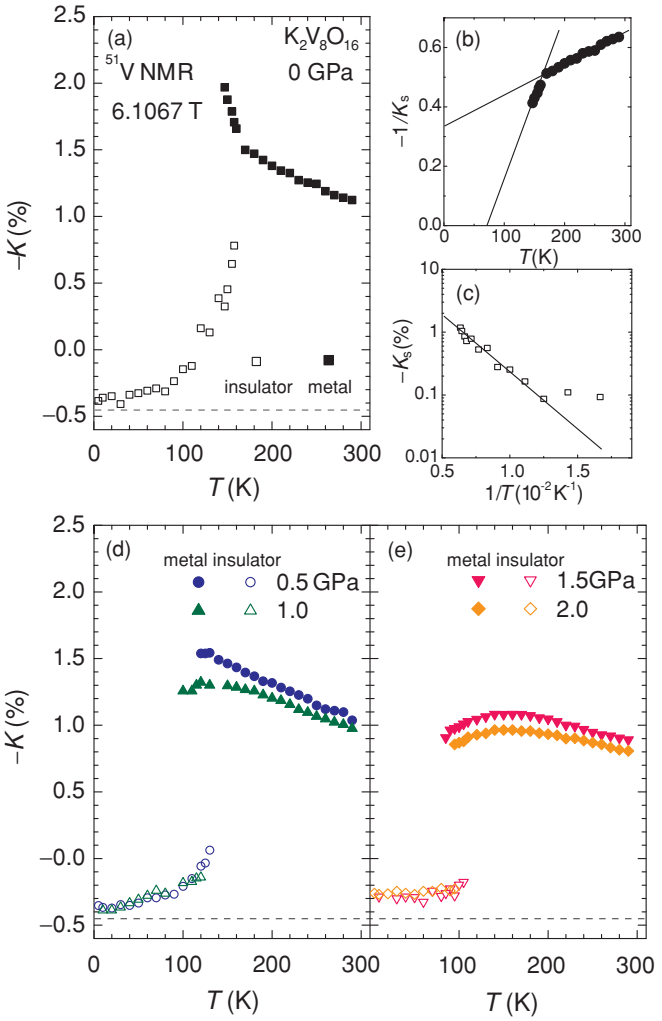

FIG. 3. (Color online) (a) Temperature dependence of the ^{51}V Knight shift $-K$ of the polycrystalline sample of $K_2V_8O_{16}$ at ambient pressure. (b) The inverse of the spin Knight shift $-1/K_s$ vs T plot in the metallic state. (c) $-K_s$ vs $1/T$ plot in the insulating state. (d), (e) Temperature dependence of $-K$ measured under pressures of 0.5, 1.0, 1.5, and 2.0 GPa. The horizontal dashed lines in (a), (d), and (e) denote $K_{\rm orb}$ evaluated from the K-$\chi_{\rm bulk}$ plot (Fig. 4) in the metallic phase at ambient pressure.

increase of $-K_s$ from the Curie-Weiss law, $-1/K_s = T - \Theta$. A linear fitting gives the Weiss temperature $\Theta_1 = -290$ K for the T range of 170–300 K, and Θ_2 = 70 K for 145–170 K. Although the meaning of Θ is not straightforward for the strongly correlated itinerant system, the result suggests that the magnetic interaction changes across 170 K. It may capture an intermediate state within the two-step transition observed by the resistivity and the x-ray-diffraction measurements.[11]

Below $T_{\rm MI}$, $-K$ of the insulating phase gradually decreases and reaches $\sim -0.4\%$, close to $-K_{\rm orb}$, which indicates that χ_s vanishes at low temperatures. This is the clear microscopic evidence for the spin-singlet formation below $T_{\rm MI}$. The activation plot of $-K_s$ in Fig. 3(c) gives a spin gap $\Delta = 182$ K. Since the insulating phase would be orbitally ordered and have the energy gap to excited orbital states, $K_{\rm orb}$ can be decreased across $T_{\rm MI}$ due to the lifting of the orbital degeneracy. Nevertheless, $K_{\rm orb}$ still remains $\sim$0.4% in

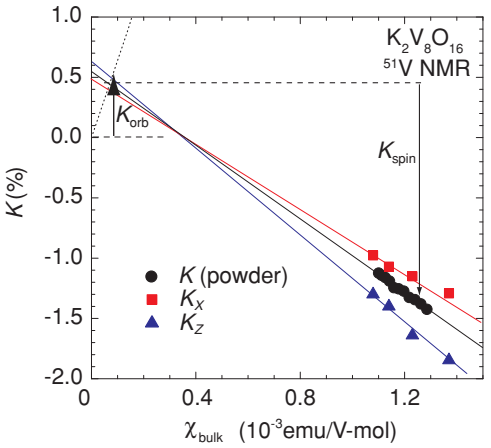

FIG. 4. (Color online) K vs magnetic susceptibility $\chi_{\rm bulk}$ plots for the polycrystalline (•) and single-crystal (△ and □) samples of $K_2V_8O_{16}$.

the insulating state, which corresponds to $\chi_{\rm orb} \sim 1 \times 10^{-4}$ emu/V mol, and is much smaller than the remaining $\chi_{\rm bulk}$ value, $\sim 5 \times 10^{-4}$ emu/V mol. It implies missing paramagnetic sites with the T-independent $\chi_s \sim 4 \times 10^{-4}$ emu/V mol, unmonitored by the Knight shift at the observed nonmagnetic site due to the too small, transferred hyperfine coupling.

The pressure effects on $-K$ are shown in Figs. 3(d) and 3(e), and the representative spectral profile at 2.0 GPa is shown in Fig. 2(b). In the metallic phase, $-K$ tends to be suppressed with increasing pressure and exhibits a broad maximum around 150 K above 1.5 GPa. The MIT is suppressed down to 85 K at $P = 1.5$ GPa, above which the decrease of $T_{\rm MI}$ levels off. The coexistence of the metallic and insulating phases persists up to 2.0 GPa, as seen in the spectral profile in Fig. 2(b). On the cooling process, the coexisting T regions are 120–150 K at 0.5 GPa, 100–140 K at 1.0 GPa, 85–105 K at 1.5 GPa, and 90–100 K at 2.0 GPa. For the insulating phase, $-K$ gradually approaches 0.3%–0.4% below 1.0 GPa, as seen at ambient pressure. In contrast, it directly goes to $\sim -0.3\%$ at $T_{\rm MI}$ above 1.5 GPa, which indicates the appearance of the nonmagnetic V sites involved in the discontinuous opening of the spin gap. As seen in Fig. 2, the linewidth tends to increase at 2 GPa ($\sim$1 MHz at 40 K) compared to ambient pressure ($\sim$0.8 MHz at 40 K).

B. Hyperfine interactions

To elucidate the mechanism of the spin-singlet formation in $K_2V_8O_{16}$, it is crucial to investigate the orbital state. NMR can probe the $3d$ orbital occupancy via the anisotropy in the magnetic and electric hyperfine coupling tensors obtained from the angle dependence of K and the quadrupole splitting frequency $\Delta\nu$, respectively.[18] The orbital-resolved NMR measurement in the $3d$ system has been mainly made on the ferromagnets such as K_2CuF_4 ($3d^9$, Ref. 19), $Lu_2V_2O_7$ ($3d^1$, Ref. 20) and $YTiO_3$ ($3d^1$, Ref. 21) or the antiferromagnet $LaTiO_3$ ($3d^1$, Ref. 22) with one electron or hole, whereas it has not been established in paramagnetic metals and nonmagnetic insulators.

The spin part of the magnetic hyperfine interaction $\mathcal{H}_{\rm mag}$ and the electric one $\mathcal{H}_{\rm el}$ between the ^{51}V nucleus (with

the nuclear spin $I = 7/2$ and the quadrupole moment $Q = -0.05 \times 10^{-24}$ cm^2) and the $3d$ electron are, respectively, expressed as[22]

$$\mathcal{H}_{\rm mag} = 2\mu_{\rm B}\gamma_{\rm N}\hbar \langle r^{-3}\rangle_{\rm mag} [-\kappa \mathbf{S}\cdot\mathbf{I} - \xi \mathbf{S}\cdot\mathsf{q}\cdot\mathbf{I}], \quad (2)$$

$$\mathcal{H}_{\rm el} = \frac{2e^2Q}{I(2I-1)}\xi \langle r^{-3}\rangle_{\rm el} [\mathbf{I}\cdot\mathsf{q}\cdot\mathbf{I}], \quad (3)$$

where $\hbar$ is the Plank's constant, κ is a parameter of the Fermi contact, $\mathbf{S}$ is the electron spin operator, and $\langle r^{-3}\rangle_{\rm mag}$ and $\langle r^{-3}\rangle_{\rm el}$ are the expectation values of r^{-3}. Here we assume that the spin-orbit coupling is negligible, as known in the vanadium oxides.[23] The first term in Eq. (2) comes from the core polarization of inner s spins, giving an isotropic shift proportional to χ_s, $K^s_{\rm iso} = A^s_{\rm iso}\chi_s/N\mu_B$ with the isotropic hyperfine coupling constant $A^s_{\rm iso} = -\kappa\mu_{\rm B}\langle r^{-3}\rangle_{\rm mag}$. The second term in Eq. (2) is the equivalent operator expression of the anisotropic dipole hyperfine interaction, where $\xi \equiv (2l+1-4S)/S(2l-1)(2l+3)(2L-1) = \frac{2}{21}$ for $3d^1$ ($l = L = 2$ and $S = 1/2$), and q is the tensor with the components $q_{ij} \equiv \frac{3}{2}(L_iL_j + L_jL_i) - \delta_{ij}\mathbf{L}^2$ $(i,j = x,y,z)$, where $\mathbf{L}$ is the total orbital angular momentum.[18,22] Here, q expressed in terms of the orbital momentum has the same form as the electric quadrupole tensor of nucleus and reflects the anisotropic distribution of $3d$ electron clouds, which can be referred to as the electron quadrupole moment. The diagonal components of q_{ij} for d_{xy} are given by $q_{zz} = -2q_{xx} = -2q_{yy} = 6$,[22] and $q_{zz} = -6$ for the sum of d^1_{yz} ($q_{xx} = -2q_{yy} = -2q_{zz} = 6$) and d^1_{zx} ($q_{yy} = -2q_{xx} = -2q_{zz} = 6$). Thus we can distinguish the two orbitals in Fig. 1(c) from the sign of q_{zz} determined by the anisotropic Knight shift. On the other hand, the maximum quadrupole frequency ν_Q is given by

$$\nu_Q = \frac{e^2Q}{7hI(2I-1)}\langle r^{-3}\rangle_{\rm el} q_{zz}, \quad (4)$$

which is evaluated as ~1.2 MHz for $|q_{zz}| = 6$. In the crystal structure of $K_2V_8O_{16}$, the z axis of the VO_6 octahedron is close to the a axis, as shown in Fig. 1(d). Taking into account the two orbital levels, the d_{xy} singlet and the d_{yz}-d_{zx} doublet, in the tetragonal crystal, the axially symmetric axis giving q_{zz} should be close to the a axis.

When the Zeeman energy is much larger than $\mathcal{H}_{\rm el}$, the ^{51}V NMR spectrum is split into equally spaced seven lines due to the nuclear quadrupole splitting for $I = 7/2$. In the paramagnetic metallic state, however, ^{51}V NMR spectra measured for the powder sample in Fig. 2 and the single-crystal sample in Fig. 5 consistently show the absence of the quadrupole splitting; ν_Q must be smaller than the linewidth, $\nu_Q \leqslant 0.5$ MHz/6. It indicates $\mathcal{H}_{\rm el} \ll \mathcal{H}_{\rm mag}$ and the negligible electric-field gradient due to the distortion of the VO_6 octahedron. Since S is proportional to the spin susceptibility for the paramagnetic state in Eq. (2), the anisotropy in the Knight shift tensor K is governed by the $3d$ orbital mainly contributing to the spin susceptibility. We determine K by measuring the angle dependence of the ^{51}V NMR spectra at $T = 160$ K for ambient pressure and 150 K for 1.5 GPa in the paramagnetic metallic state, shown in Figs. 5(a) and (b), respectively. In the rotation around the c axis, the two V sites in Fig. 1 that are orthogonal to each other become inequivalent under the magnetic field. Although the spectra from the two V sites overlap due to the broad linewidth and the small shift, we could separate the two by utilizing the difference in the optimum pulse condition and T_2. We plot K defined by a peak position of the spectrum versus the rotation angle θ in Figs. 5(c) and 5(d). The plots are well fitted to two sets of sinusoidal curves,

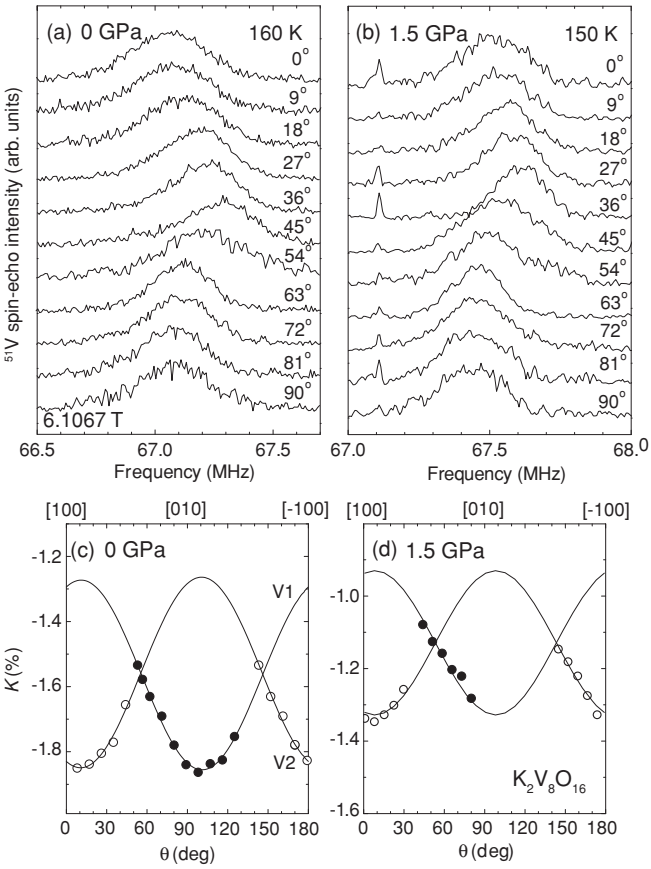

FIG. 5. (a), (b) Angle dependence of ^{51}V NMR spectra and (c), (d) K with H_0 rotated in the c plane of the single crystal of $K_2V_8O_{16}$ at ambient pressure and 1.5 GPa. The spectral intensity is normalized by the maximum value at each angle.

$$K(\theta',\phi) = K_X\sin^2\theta'\cos^2\phi + K_Y\sin^2\theta'\sin^2\phi + K_Z\cos^2\theta', \quad (5)$$

where (K_X, K_Y, K_Z) are the principal components of K, $\phi = 0$, and $\theta' = \theta - \alpha_0$ with a constant α_0.[24] A relative constant phase of 90° between the two curves satisfies the tetragonal symmetry of the crystal. Furthermore, $-K$ has a maximum or a minimum at the direction close to the a axis, as expected from the directions of VO_6 octahedra. Hence the spectral weight is regarded as mainly coming from one of the two V sites. Together with the data of the ac rotation ($\phi = 90°$) and the axial symmetry, we obtain $(K_X, K_Y, K_Z) = (-1.25 \pm 0.1, -1.25 \pm 0.1, -1.85 \pm 0.1\%)$ at ambient pressure, and $(-0.93 \pm 0.1, -0.93 \pm 0.1, -1.33 \pm 0.1\%)$ at 1.5 GPa, where the principal Z axis is nearly parallel to the a axis.

From the K-$\chi_{\rm bulk}$ plots in Fig. 4, K is decomposed into the spin part $\mathsf{K_s}$ and the orbital part $\mathsf{K}_{\rm orb} = (0.40 \pm 0.1, 0.40 \pm 0.1, 0.50 \pm 0.1\%)$. The linearity in the K-$\chi_{\rm bulk}$ plot

gives $A^s_Z = -97$ kOe/μ_B and $A^s_{X,Y} = -70$ kOe/μ_B, leading to the axially symmetric part $A^s_{ax} = 2(A^s_Z - A^s_{X,Y})/3 = -18$ kOe/μ_B and the isotropic part $A^s_{iso} = (A^s_Z + 2A^s_{X,Y})/3 = -79$ kOe/μ_B at ambient pressure. The orbital state can be measured from $A^s_{ax} = -\xi\mu_B \langle r^{-3}\rangle_{mag} q_{zz}$, which is evaluated as -132 kOe/μ_B for $3d^1$ using the free V^{4+} ion value of $\langle r^{-3}\rangle$, $\langle r^{-3}\rangle_{FI} = 3.684$ a.u. We obtained $q_{zz} = 0.82$ by using $\langle r^{-3}\rangle_{FI}$.

The positive value is consistent with the predominant d_{xy} contribution. Although q_{zz} may be reduced by a factor of ~ 2 due to the hybridization to O $2p$ orbitals and the excess 0.25 electrons, the value of $q_{zz} = 0.82$ corresponds to only 14% of the full $3d^1$ quadrupole moment. It manifests significant mixing of the d_{yz} and d_{zx} components.

To evaluate the mixing ratio, we introduce an anisotropy parameter A^s_{ax}/A^s_{iso} that can cancel out $\langle r^{-3}\rangle_{mag}$, depending on the V valence and the orbital state. A^s_{ax}/A^s_{iso} is obtained as 0.11, in good agreement with $K^s_{ax}/K^s_{iso} = 0.12$ independently evaluated at 160 K from $\mathsf{K}_s = (-1.65 \pm 0.1, -1.65 \pm 0.1, -2.35 \pm 0.1\%)$, giving $K^s_{iso} = -1.88 \pm 0.1\%$ and $K^s_{ax} = -0.23 \pm 0.1\%$. In comparison with a theoretical value, $A^s_{ax}/A^s_{iso} = \frac{2}{7\kappa} = 0.57$ for d^1_{xy} and $-\frac{2}{7\kappa} = -0.57$ for the d_{yz}-d_{zx} admixture by using a standard $\kappa = 0.5$, the mixing ratio is estimated as $d_{xy} : d_{yz} : d_{zx} = 3 : 2 : 2$. This is consistent with a band calculation in the generalized gradient approximation showing the narrower d_{xy} band than the d_{yz} and d_{zx} bands,[25] which can give a larger χ_s of d_{xy} than that of d_{yz}-d_{zx}. At 1.5 GPa, we obtain $\mathsf{K}_s = (-1.33 \pm 0.1, -1.33 \pm 0.1, -1.83 \pm 0.1\%)$, assuming the same K_{orb} as that at ambient pressure, which gives $K^s_{iso} = -1.50 \pm 0.1\%$, $K^s_{ax} = -0.16 \pm 0.1\%$, and $K^s_{ax}/K^s_{iso} = 0.11$. Consequently, the mixing ratio of the t_{2g} orbitals in χ_s is nearly independent of pressure that suppresses the net χ_s. It suggests the band structure is robust against pressure, although the nature of the MIT changes at high pressures.

In the insulating phase of $K_2V_8O_{16}$, we still do not observe the quadrupole splitting even for the single-crystal measurement, as shown in Fig. 6. The temperature dependence of the NMR spectrum in Fig. 6(a) is consistent with the result of the polycrystalline sample. The linewidth becomes much broader compared to the metallic state, despite the vanishing K_s from the on-site $3d$ spins. Since several inequivalent V sites appear in the insulating phase having the charge and orbital orders, the single NMR spectrum consists of the several spectra with the nuclear quadrupole splitting and K_{orb} different from each other. However, the broad spectrum cannot be explained by the small difference of K_{orb}. Hence the linewidth is dominated by $\mathcal{H}_{el} \gg \mathcal{H}_{mag}$, where the several sets of equally spaced seven lines merge due to the broadening.

We observed the strong angle dependence in the linewidth and intensity at 20 K, as shown in Fig. 6(b). The linewidth exhibits a maximum at the a axis and a minimum around 45°. Since 75% of the V ions are V^{4+} with the $3d^1$ orbital order, the angular dependence of the spectrum is expected to reflect the $3d^1$ orbital state. The symmetry lowering into the monoclinic lattice can lift the degeneracy of d_{yz} and d_{zx}. However, the d_{yz} or d_{zx} orbital order cannot give the anisotropy of the electric-field gradient in the c-axis rotation. On the other hand, the q_{zz} direction is the a axis for the d_{xy} orbital order, which is consistent with the experimental result. The linewidth is expected to have a minimum at the magic angle of 54.7°,

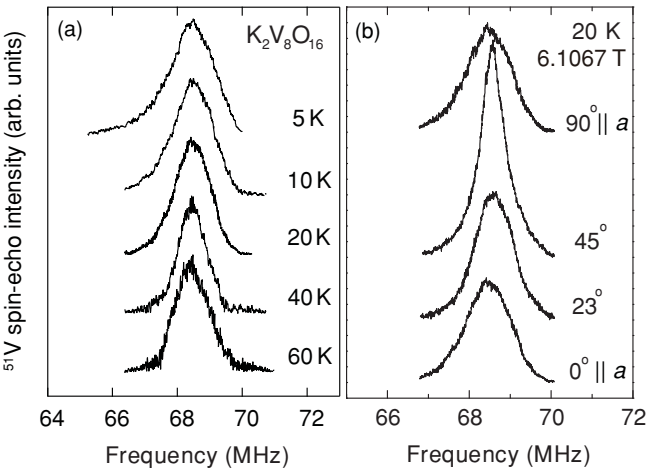

FIG. 6. (a) Temperature dependence of the ^{51}V NMR spectra in the single crystal of $K_2V_8O_{16}$ with a magnetic field of 6.1067 T along the a axis at ambient pressure. (b) Angle dependence of the ^{51}V NMR spectra at 20 K in the c plane.

where $\Delta\nu = \nu_Q(3\cos^2\theta - 1) = 0$, which is also consistent with the spectral narrowing around 45°. The edge width of the spectrum at the a axis is no more than 3 MHz, i.e., $\nu_Q \leqslant 3$ MHz/6 = 0.5 MHz, giving $|q_{zz}| \leqslant 2.5$. The d_{xy} orbital order is consistent with the MIT driven by the electron correlation, as highlighted in the enhancement of the spin susceptibility of d_{xy} in the metallic state.

C. Dynamical spin susceptibility

Dynamical properties of the phase transition can be unusual in the frustrated systems. As shown in Fig. 7, $1/T_1T$ weakly depends on T in the metallic phase, and somewhat deviates from the T-independent Korringa's law expected in a weakly correlated metal. Entering into the insulating phase, $1/T_1T$ increases abruptly, despite the decrease of $-K$, with a peak around 140 K. The enhancement is also observed in $1/T_1$ and $1/T_2$, as shown in the inset of Fig. 7. It cannot be a sign of the magnetic order because no broadening of the NMR spectra is observed across 140 K. A possible reason is the enhancement of spin, charge, and orbital fluctuations accompanied by MIT. Although we cannot experimentally distinguish these fluctuations, it is noted that the decrease in $1/T_2$ is retarded by 20–30 K compared to the decrease of $1/T_1$, which implies the frequency dependence of the fluctuations with the slow dynamics, as observed in $PrBa_2Cu_4O_8$ (Ref. 26) and θ-$(ET)_2CsZn(SCN)_4$ (Ref. 27) having charge frustration. Below 40 K, $1/T_1T$ increases again. It also cannot be a precursor of the magnetic transition, because no anomaly is observed in $1/T_1$ and $1/T_2$ at low temperatures.

Application of pressure suppresses $1/T_1T$ in the metallic state, as shown in Fig. 8. It corresponds to the suppression of $-K$ under pressure, although the broad peak of $-K$ above 1.5 GPa is not observed in $1/T_1T$. Just below T_{MI}, an enhancement of $1/T_1T$ appears at 0.5 GPa, as observed at ambient pressure, but tends to be suppressed at 1.0 GPa. The decrease of $1/T_1T$ and $1/T_2$ is smooth below 1 GPa, consistent with the gradual opening of the spin gap. Above 1.5 GPa, however, $1/T_1T$ drops discontinuously at T_{MI}, coinciding with

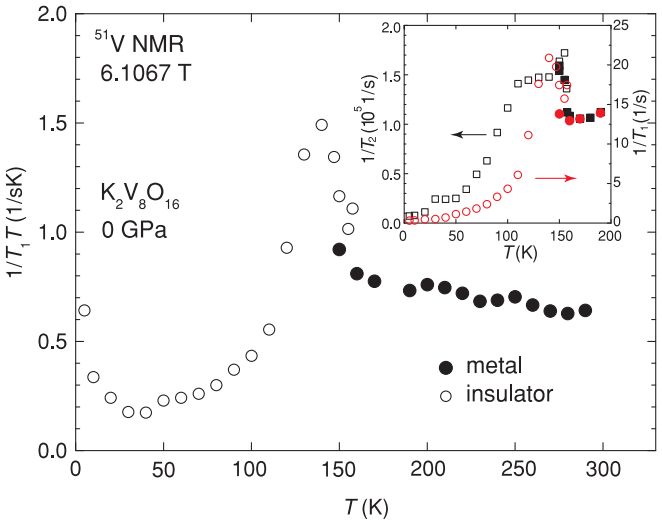

FIG. 7. (Color online) Temperature dependence of the ^{51}V nuclear spin-lattice relaxation rate divided by temperature, $1/T_1T$, for the polycrystalline sample of $K_2V_8O_{16}$ at ambient pressure. The inset shows the spin-echo decay rate $1/T_2$ (left axis) and $1/T_1$ (right axis).

a drop of $1/T_2$. It also corresponds to the abrupt decrease in K at T_{MI} and confirms the appearance of the nonmagnetic V sites. At low temperatures, an increase of $1/T_1T$ becomes prominent and close to the Curie law $1/T_1T \sim 1/T$. It suggests the presence of paramagnetic spins that would be more sensitively reflected in $1/T_1$ than K. A large amount of paramagnetic spins have been actually observed in χ_{bulk} above 1 GPa.[17] However, no indication of the long-range magnetic order is observed in $1/T_1T$ and $1/T_2$ down to 5 K.

IV. DISCUSSION

A. Spin correlation in the metallic phase

The highly enhanced χ_s with the Curie-Weiss-like T dependence remains a typical enigma of the strongly correlated metal. The origin has been interpreted from both the Fermi-liquid picture and the strongly localized picture, although no consensus has been made for 3d transition metal oxides with orbital degrees of freedom. A measure of the weakly correlated Fermi liquid is known as the modified Korringa's relation,[28]

$$\frac{1}{T_1TK_s^2} = \frac{4\pi k_B}{\hbar}\left(\frac{\gamma_N}{\gamma_e}\right)^2 K(\alpha), \qquad (6)$$

where a constant parameter $K(\alpha)$ is less (larger) than unity in the presence of a weakly ferromagnetic (antiferromagnetic) correlation, and γ_N (γ_e) is the nuclear (electron) gyromagnetic ratio. As shown in Fig. 9, $K(\alpha)$ monotonously decreases from unity on cooling at ambient pressure. The behavior is incompatible with the Fermi-liquid picture. On the other hand, $(T_1TK_s)^{-1}$ is almost independent of T, which does not contradict the weakly ferromagnetic metal within the 3D self-consistent renormalization (SCR) theory giving the Curie-Weiss $1/T_1T$ and $-K_s$.[29] At high temperatures, however, $\Theta_1 < 0$ in χ_s is inconsistent with the SCR theory. At least in the T range with $\Theta_2 > 0$, $K(\alpha) < 1$ can be explained by the ferromagnetic correlation. More generally, the direct

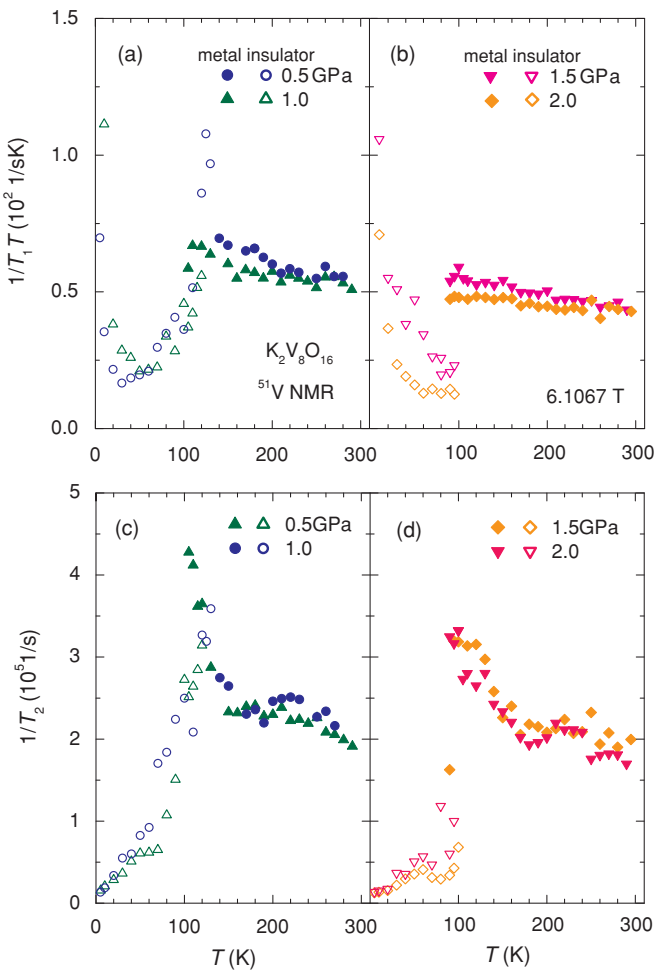

FIG. 8. (Color online) Temperature dependence of $1/T_1T$ of the polycrystalline sample of $K_2V_8O_{16}$ under pressures of (a) 0.5 and 1.0 GPa, and (b) 1.5 and 2.0 GPa. $1/T_2$ at (c) 0.5 and 1.0 GPa, and (d) 1.5 and 2.0 GPa.

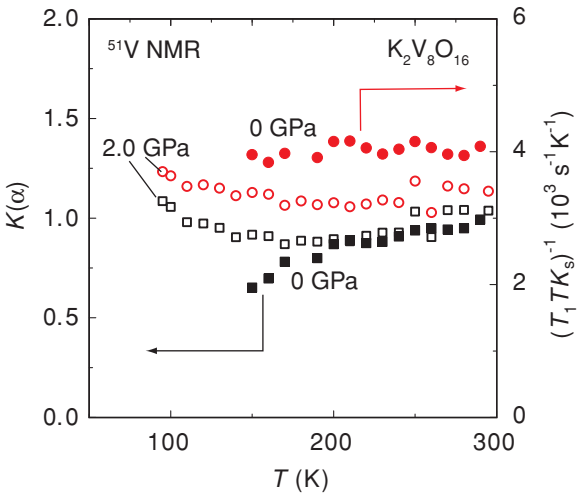

FIG. 9. (Color online) Temperature dependence of $K(\alpha)$ (left axis) and $-1/T_1TK_s$ (right axis) in the polycrystalline sample of $K_2V_8O_{16}$ at ambient pressure and 1.5 GPa.

scaling between $1/T_1T$ and χ_s means that the imaginary part of the dynamical spin susceptibility at the wave vector $\mathbf{q}$ and the NMR frequency ω_N, $\Sigma_{\mathbf{q}}\chi''(\mathbf{q},\omega_N)$, is independent of $\mathbf{q}$. Namely, the spin fluctuations are spatially localized without short-range correlations. The geometrical frustration may play a crucial role in suppressing the spin correlation.

As pressure increases up to 2.0 GPa, $K(\alpha)$ becomes close to unity but still weakly depends on temperature. It suggests that the system becomes more like a standard Fermi liquid with the spin fluctuations governed by the density of states. From the $-K_s$ value at 2.0 GPa, χ_s is evaluated as $\sim 1 \times 10^{-3}$ emu/V mol by using $A_s = -79$ kOe/μ_B. If we assume χ_s governed by the density of states, it is enhanced by a factor of 8, compared to the free-electron value $\chi_s = 1.2 \times 10^{-4}$ emu/V mol by using the calculated density of states, 2.8 states/eV V.[25] It suggests the strong correlation effect in the metallic phase. Nevertheless, no apparent magnetic correlation is observed in both $K(\alpha)$ and $(T_1TK_s)^{-1}$, which corresponds to the absence of the magnetic order in the ground state.

B. Magnetic ground states

Finally we discuss the macroscopic and microscopic features in the low-pressure insulating (LI) phase and the high-pressure (HI) one. Figure 10 shows the P-T phase diagram obtained from the NMR measurements. T_{MI} refers to the NMR spectrum on the cooling process. The paramagnetic metallic (PM) phase is regarded as the incoherent bad metal, at least at low pressures, and approaches a coherent metal with increasing pressure, as discussed above. The insulating phases include majority nonmagnetic sites as revealed by the ^{51}V NMR Knight shift measurements at $P \leqslant 2$ GPa. The K, $1/T_1T$, and $1/T_2$ results consistently demonstrate the qualitatively different nature in the LI phase at $P \leqslant 1$ GPa and the HI phase at $P \geqslant 1.5$ GPa.

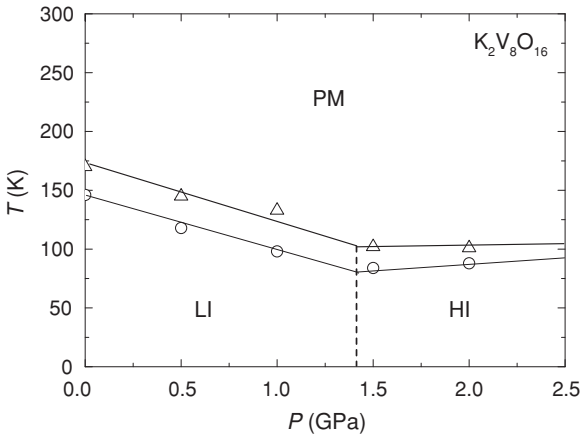

FIG. 10. Pressure-temperature phase diagram of $K_2V_8O_{16}$. The phase-transition temperatures marked by △ and ○ are determined as the temperature where the insulating phase appears and the metallic disappears, respectively, in the ^{51}V NMR spectra. The phase diagram is classified into three regions, paramagnetic metal (PM), low-pressure insulator (LI), and high-pressure insulator (HI). The detail of each phase is described in the text.

From a thermodynamic point of view, the slope of the first-order line is expressed by the Clausius-Clapeyron relation $dT/dP = \Delta V/\Delta S$, where ΔV and ΔS are the difference of volume and entropy, respectively, between the insulating and metallic phases. Since ΔS should be always negative owing to the nonmagnetic ground state, the negative dT/dP in the low-pressure range indicates the positive ΔV. This is consistent with the volume expansion (0.14%) at T_{MI}, as observed by the x-ray diffraction.[11] This is also compatible to the correlation-driven MIT, which would accompany the volume expansion. The suppression of T_{MI} with pressure is well known in the MIT systems, e.g., V_2O_3 (Ref. 30) and β-$Na_{0.33}V_2O_5$ (Refs. 31, 32). In contrast, the slightly positive dT/dP slope of the PM-HI boundary points to the negative ΔV, i.e., a shrinking of the lattice in the HI phase. It suggests the strong lattice dimerization or clusterization, which may give the strong first-order transition of the spin-singlet formation observed as the discontinuous drop of K, $1/T_1T$, and $1/T_2$ at T_{MI} above 1 GPa. The anomalously robust HI phase against the reduction of electron correlations can be stabilized by the energy gain of the spin gap, similar to the Peierls transition.

From a microscopic point of view, the magnetic ground state at ambient pressure has been investigated only from the strong correlation limit, which would involve the charge and orbital orders due to the fractional band filling of $3d^{1.25}$. There are now two charge-order models which satisfy the superlattice with a period of $\sqrt{2}a \times \sqrt{2}a \times 2c$.[11] One is the separation chain model; with one V^{3+} chain and three V^{4+} chains in the two double chains, forming the spin dimerization along the chain.[11] Another is the mixed spin model; with the spin-singlet pairs and the ferromagnetically coupled paramagnetic spins in the same double chain.[16] In the former model, the d_{xy} orbital order is favorable to form the spin singlet along the V^{4+} chains, whereas the d_{yz} or d_{zx} orbital is used for the singlet pairs in the latter model. Our observation of the d_{xy} character in the metallic and insulating phases is compatible to the separation chain model. There is, however, remaining frustration in the arrangement of the 25% V^{3+}-like sites, which can be paramagnetic. Although the NMR spectra from the magnetic sites would be wiped out, the direct d-d transfer path, if any, should give a significant paramagnetic Knight shift at the nonmagnetic site via transferred hyperfine interactions, as observed in $Ba_2V_{13}O_{22}$.[33] The absence of the Knight shift from the remaining paramagnetic spins observed in χ_{bulk} suggests that the magnetic ion sites are spatially or orbitally separated from the nonmagnetic sites, as seen in AlV_2O_4.[34]

In the LI phase, the expected T-independent spin susceptibility of the paramagnetic sites should arise from the low-dimensional antiferromagnetic fluctuations, which are possible when V^{3+} sites form the 1D chain. In the HI phase, χ_{bulk} exhibits the Curie-Weiss behavior with a considerably large effective moment $P_{eff} \sim 1\mu_B$ and the Weiss temperature of -5, which is ~ -20 K above 1 GPa.[17] It indicates the presence of nearly isolated paramagnetic spins, which was not observed by the Knight shift. The isolation of the paramagnetic sites coincides with the tightening of the spin-singlet formation. The drastic change between the LI and HI phases can involve the orbital switching. The possible scenario is the suppression of the correlation-induced orbital order in

the HI phase, as theoretically suggested in the spinel oxides.[35] The theoretical approach from the orbitally induced Peierls transition in the hollandite system is an interesting issue for future research. At least for the band calculation, there are both 1D-like and closed Fermi surfaces, owing to the significant interactions between the double chain,[25] which cannot vanish the whole Fermi surface by the conventional 1D nesting.

V. CONCLUSION

The metal-insulator transition in $K_2V_8O_{16}$ was investigated by the ^{51}V NMR measurements at ambient pressure and under pressure. We gave microscopic evidence for the spin-singlet formation at pressures up to 2 GPa. Across the critical pressure of 1–1.5 GPa, the formation of the spin singlet becomes robust against pressure, as reflected in the positive slope of the first-order line in the pressure-temperature phase diagram, as well as the drop of the Knight shift and the nuclear relaxation rates at T_{MI}. It implies a pressure-induced switching of the spin-singlet texture. We determined the hyperfine coupling tensors in the paramagnetic metallic state at ambient pressure and 1.5 GPa. The anisotropy of the tensor showed the significant orbital mixing of the d_{xy} band and the d_{yz}/d_{zx} one, but the slightly predominant contribution of d_{xy} to the spin susceptibility. The anisotropic electric-field gradient in the insulating phase is consistent with the d_{xy} orbital order for the V^{4+} ions. The spin fluctuations observed by the nuclear spin-lattice relaxation rate are spatially localized without magnetic correlation. It may manifest in the unusual nature of the geometrical frustration.

ACKNOWLEDGMENTS

We appreciate fruitful discussion with Y. Ohta and Y. Motome. We also thank S. Inoue for technical assistance. This work was financially supported by the Grant-in-Aid for Scientific Research on Priority Areas, Novel State of Matter Induced by Frustration (Grant No. 22014006), Special Coordination Funds for Promoting Science and Technology from the MEXT, and also by Grants-in-Aid for Scientific Research (Grants No. 18104008, No. 19340097, and No. 19740224) from the JSPS.

[1] S. H. Lee, H. Takagi, D. Louca, M. Matsuda, S. Ji, H. Ueda, Y. Ueda, T. Katsufuji, J. H. Chung, S. Park, S. W. Cheong, and C. Broholm, J. Phys. Soc. Jpn. **79**, 011004 (2010).
[2] C. Lacroix, J. Phys. Soc. Jpn. **79**, 011008 (2010).
[3] A. A. Nersesyan, A. O. Gogolin, and F. H. L. Essler, Phys. Rev. Lett. **81**, 910 (1998).
[4] T. Hikihara, T. Momoi, A. Furusaki, and H. Kawamura, Phys. Rev. B **81**, 224433 (2010).
[5] E. H. Kim, Ö. Legeza, and J. Sólyom, Phys. Rev. B **77**, 205121 (2008).
[6] K. Okunishi, J. Phys. Soc. Jpn. **77**, 114004 (2008).
[7] D. V. Dmitriev and V. Y. Krivnov, Phys. Rev. B **77**, 024401 (2008).
[8] D. N. Sheng, O. I. Motrunich, and M. P. A. Fisher, Phys. Rev. B **79**, 205112 (2009).
[9] L. N. Bulaevskii, C. D. Batista, M. V. Mostovoy, and D. I. Khomskii, Phys. Rev. B **78**, 024402 (2008).
[10] H. Kato, T. Waki, M. Kato, K. Yoshimura, and K. Kosuge, J. Phys. Soc. Jpn. **70**, 325 (2001).
[11] M. Isobe, S. Koichi, N. Kouno, J. Yamaura, T. Yamauchi, H. Ueda, H. Gotou, T. Yagi, and Y. Ueda, J. Phys. Soc. Jpn. **75**, 073801 (2006).
[12] K. Hasegawa, M. Isobe, T. Yamauchi, H. Ueda, J. I. Yamaura, H. Gotou, T. Yagi, H. Sato, and Y. Ueda, Phys. Rev. Lett. **103**, 146403 (2009).
[13] K. Yamaura, M. Arai, A. Sato, A. B. Karki, D. P. Young, R. Movshovich, S. Okamoto, D. Mandrus, and E. Takayama-Muromachi, Phys. Rev. Lett. **99**, 196601 (2007).
[14] O. Pieper, B. Lake, A. Daoud-Aladine, M. Reehuis, K. Prokeš, B. Klemke, K. Kiefer, J. Q. Yan, A. Niazi, D. C. Johnston, and A. Honecker, Phys. Rev. B **79**, 180409R (2009).
[15] N. Katoh, J. Phys. Soc. Jpn. **68**, 258 (1999).
[16] S. Horiuchi, T. Shirakawa, and Y. Ohta, Phys. Rev. B **77**, 155120 (2008).
[17] T. Yamauchi, H. Ueda, M. Isobe, and Y. Ueda (private communication).
[18] A. Abragam and B. Bleaney, *Electron Paramagnetic Resonance of Transition Ions* (Oxford University Press, London, 1970).
[19] H. Kubo, N. Kaneshima, and K. Hirakawa, J. Phys. Soc. Jpn. **41**, 1165 (1976).
[20] T. Kiyama, T. Shiraoka, M. Itoh, L. Kano, H. Ichikawa, and J. Akimitsu, Phys. Rev. B **74**, 184422 (2006).
[21] T. Kiyama, H. Saitoh, M. Itoh, K. Kodama, H. Ichikawa, and J. Akimitsu, J. Phys. Soc. Jpn. **74**, 1123 (2005).
[22] T. Kiyama and M. Itoh, Phys. Rev. Lett. **91**, 167202 (2003).
[23] T. Ohama, H. Yasuoka, M. Isobe, and Y. Ueda, J. Phys. Soc. Jpn. **66**, 3008 (1997).
[24] C. P. Slichter, *Principles of the Magnetic Resonance*, 3rd ed. (Springer-Verlag, Berlin, 1990).
[25] M. Sakamaki, S. Horiuchi, T. Konishi, and Y. Ohta, e-print arXiv:0811.4338 (to be published).
[26] S. Fujiyama, M. Takigawa, and S. Hiroi, Phys. Rev. Lett. **90**, 147004 (2003).
[27] R. Chiba, K. Hiraki, T. Takahashi, H. M. Yamamoto, and T. Nakamura, Phys. Rev. Lett. **93**, 216405 (2004).
[28] T. Moriya, J. Phys. Soc. Jpn. **18**, 516 (1963).
[29] T. Moriya, J. Magn. Magn. Mater. **100**, 261 (1991).
[30] D. B. McWhan, A. Menth, J. P. Remika, W. F. Brinkman, and T. M. Rice, Phys. Rev. B **7**, 1920 (1973).
[31] T. Yamauchi and Y. Ueda, Phys. Rev. B **77**, 104529 (2008).
[32] T. Suzuki, I. Yamauchi, Y. Shimizu, M. Itoh, N. Takeshita, C. Terakura, H. Takagi, Y. Tokura, T. Yamauchi, and Y. Ueda, Phys. Rev. B **79**, 081101 (2009).
[33] J. Miyazaki, K. Matsudaira, Y. Shimizu, M. Itoh, Y. Nagamine, S. Mori, J. E. Kim, K. Kato, M. Takata, and T. Katsufuji, Phys. Rev. Lett. **104**, 207201 (2010).
[34] Y. Shimizu, M. Tanaka, M. Itoh, and T. Katsufuji, Phys. Rev. B. **78**, 144423 (2008).
[35] D. I. Khomskii and T. Mizokawa, Phys. Rev. Lett. **94**, 156402 (2005).